Int. J. Electrochem. Sci., 13 **(2018)** 12320 – 12330, doi: 10.20964/2018.12.24

International Journal of
ELECTROCHEMICAL
SCIENCE
www.electrochemsci.org

Facial Synthesis of 3D MnO_2 Nanofibers Sponge and Its Application in Supercapacitors

Chuanyun Wan[1,*], *Haiyan Shen*[2], *Xiangrong Ye*[2], *Fanhong Wu*[1]

[1] School of Chemical and Environmental Engineering, Shanghai Institute of Technology, Haiquan Road 100, 201418，Shanghai, People's Republic of China,
[2] Key Laboratory of the Ministry of Education for Advanced Catalysis Materials, College of Chemistry and Life Sciences, Zhejiang Normal University, Jinhua, 321004, Zhejiang, People's Republic of China,
[*]E-mail: cywan@sit.edu.cn

Received: 28 June 2018 / *Accepted:* 21 Sepember 2018 / *Published:* 5 November 2018

Mesoporous Al_2O_3 template was facially constructed by hydrolysis of aluminum nitrate solution, and 3D MnO_2 foam was fabricated by redox reaction of Mn^{2+} and MnO_4^- in the nanoholes of Al_2O_3 template, followed by sacrificial dissolution of the Al_2O_3 matrix. The as-prepared 3D MnO_2 sponge is composed of cross-linked worm-like nanofibers which promise enhanced charge transfer capability. The specific surface area and porosity of the MnO_2 sponge is affected by the concentration of Mn^{2+} ion when the pores of Al_2O_3 template were immersed, and higher specific surface area, higher pore volume and hence better electrochemical performance were developed at lower Mn^{2+} concentration. When 0.02mol L^{-1} of Mn^{2+} solution was used to immerse the Al_2O_3 template, a specific capacitance of 215.3F g^{-1} can be achieved for the resultant 3D MnO_2 sponge in 1 mol L^{-1} Na_2SO_4 aqueous electrolyte at 2mV s^{-1} scan rate, and all as-prepared 3D MnO_2 sponges provide good long-term charging/discharging stability with approximate 96% retention of capacitance at 5mV s^{-1} scan rate after 2000 cycles, showing that the facially synthesized 3D MnO_2 sponge is a promising electrode material for supercapacitor.

Keywords: 3D MnO_2 sponge; nanofiber; mesoporous Al_2O_3 template; supercapacitor.

1. INTRODUCTION

The ever-increasing ecological issues and energy crisis have triggered worldwide searching for renewable energy sources and better energy-storage systems demanded by a variety of application, including portable electronics, power supply devices and electric vehicles[1-4]. Electrochemical supercapacitors, as a branch of energy-storage devices, have attracted tremendous research interest due

to their high power density, fast charging/discharging rate and long cycle life [5,6]. The performance of electrochemical supercapacitors, to a great extent, is controlled by the structural and electrochemical properties of electrode materials. Typical electrode materials for electrochemical supercapacitors include carbon, transition metal oxide and conductive polymer[7-9]. Although carbon materials with high surface area exhibit high specific power and excellent cycle life in electrical double layer capacitor and have been successfully commercialized in practice[10, 11], their electrodes usually provide low capacitance values[11, 12].

MnO_2, a transition metal oxide, has been considered as one of the most prominent electrode materials for electrochemical capacitor due to its low cost and high theoretical capacitance (1370 F g^{-1})[13]. Its faradaic pseudocapacitance arises through two mechanisms, adsorption/desorption of ions on the interface between electrolyte and electrode during charging/discharging, and the Faraday reactions on the active surface of MnO_2 [9, 11, 12, 14]. However, the poor electrical conductivity of MnO_2 determines that a fast redox process in general could only occur on the outer surface of the material [15]. Hence, nanosization of MnO_2 to shorten the transportation distance of electrons from electrolytes to the inner phase of the material has become a common strategy to improve the conductivity as well as the performance of MnO_2 in supercapacitor electrodes[8, 16]. Various MnO_2 nanomaterials (nanorod [16], nanoflower [16-18], three-dimensional (3D) nanocomposite [13, 19-21], nanowire [22], etc.) have been reported to upgrade the electrochemical performance of MnO_2-based supercapacitors. Furthermore, considering the instability and collapsing easiness of one-dimensional/two-dimensional architectures [23, 24], MnO_2 nanocomposites with 3D architectures have been paid more attention [13, 19, 20, 25]. In this context, we report a simple and cost-effective method to prepare a three-dimensional MnO_2 nanostructured sponge material with high charge transfer capability and excellent electrochemical performance for potential application in supercapacitor electrodes. Herein mesoporous Al_2O_3 was synthesized by hydrolyzing aluminum nitrate solution and used as sacrificial template.

2. EXPERIMENTAL

2.1 Reagents and synthesis

All reagents were analytical-grade and used as received without purification. The mesoporous alumina sponge was prepared by the similar process described in literature[26]. 0.1mol L^{-1} $(NH_4)_2CO_3$ aqueous solution was dropped slowly into 50mL of 0.2mol L^{-1} $Al(NO_3)_3$ solution with vigorous magnetic stirring until a sudden formation of transparent gel took place and the stirring was stopped. The gel was aged at 30 ^{0}C for 24h, and then heated at 100 ^{0}C for 10h. Afterwards, the obtained solid was transferred to a furnace and heat-treated at 300 ^{0}C for 10h in air at a heating rate of 5 ^{0}C min^{-1}. The as-prepared alumina was ready for serving as sacrificial template to prepare 3D MnO_2 sponge.

3D MnO_2 sponge was fabricated according to the following steps. Alumina sponge was soaked in $MnCl_2$ solution (0.02mol L^{-1}, 0.1mol L^{-1} and 1mol L^{-1}, respectively) and stirred for 2h. The alumina was then separated by filtration and redispersed in 0.01mol L^{-1} $KMnO_4$ aqueous solution for 2h to form MnO_2 in Al_2O_3 sponge matrix. The MnO_2/Al_2O_3 composite was collected and washed three times with

deionized water. Finally, the alumina containing MnO_2 was immersed in 2mol L^{-1} NaOH solution at 80 ^{0}C to dissolve Al_2O_3 matrix completely, and the black-brown 3D MnO_2 sponge residue was collected by filtration, washed with deionized water and dried at 60 ^{0}C for 12h in a vacuum oven. The overall fabrication flow of 3D MnO_2 sponge is charted in Fig.1.

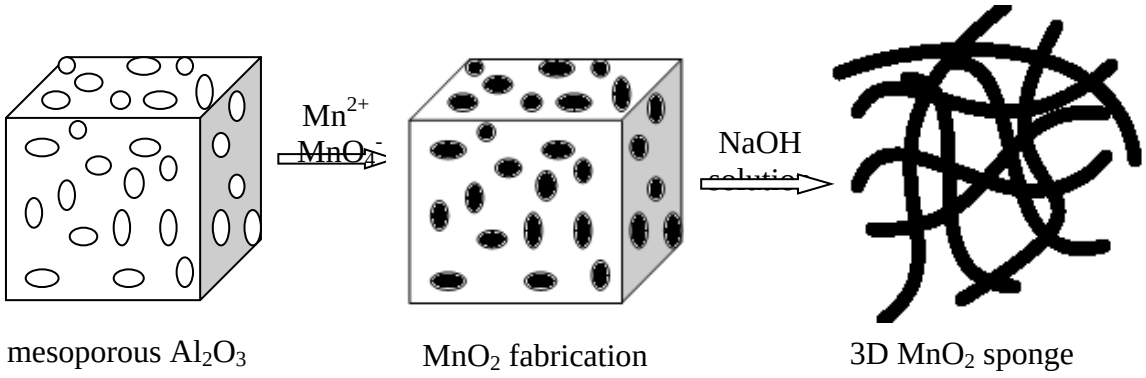

Figure 1. Schematic illustration of the synthesis of 3D MnO_2 sponge

2.2 Material characterization and electrochemical measurements

The structure and morphology of the as-synthesized MnO_2 samples were characterized by X-ray powder diffraction (XRD, PANalytical Almelo, The Netherlands, CuKα anode, λ=1.54187Å), scanning electron microscopy(SEM, FEI Quanta 200 EEG) and transmission electron microscopy(TEM, Hitachi 600, Japan). Nitrogen adsorption and desorption experiments were carried out at 77.3K with a Micrometritics ASAP 2020. The pore size distribution was calculated by the Barrett-Joyner-Halenda (BJH) method.

The electrochemical behavior of the obtained samples was measured using three-electrode system at room temperature on a GAMRY electrochemical working station (Gamry Reference 600$^+$ Instruments, USA). To form working electrodes, 65 wt.% of as-prepared MnO_2 sponge powder, 25 wt.% of super P (conductive carbon), 10 wt.% of poly-(tetrafuloroethylene) (PTFE) binder and small amount of ethanol were mixed homogenously and then pressed onto nickel foam current collectors. The typical loading of the MnO_2 material was ca. 10 mg cm^{-2}. The electrodes were dried at 50 ^{0}C for 10h in a vacuum oven. Saturated calomel electrode (SCE) and platinum foil were used as reference electrode and counter electrodes, respectively. The working electrolyte was 1 mol L^{-1} Na_2SO_4 solution. Electrochemical studies were performed by cyclic voltammetry (CV), chronopotentiometry (CP) and electrochemical impedance spectroscopy (EIS) techniques.

The specific capacitance (C F g^{-1}) of a single electrode is calculated from CV curves by the formula [8]

$$C= (\int i\, dv) / (2\, v\, \Delta V\, m)$$

Where i (A g^{-1}) is the current density, v (mV s^{-1}) is the potential scan rate. △V(V) is the applied potential window, and m is the mass of MnO_2 in working electrode.

3. RESULTS AND DISCUSSION

The morphological analysis of the as-prepared Al_2O_3 template was performed in terms of SEM and the image is shown in Fig.2a. One can observe that massive white Al_2O_3 monoliths are an aggregation of nanoparticles. The N_2 adsorption-desorption isotherm of Al_2O_3 template is shown in Fig.2b, with the pore size distribution calculated by BJH method as inset. Obviously, the Al_2O_3 monolithic skeleton contains mesopores with relatively uniform pore size around 4.0 nm, therefore very thin nanostructure could be expected to generate using such Al_2O_3 sample as sacrificial template.

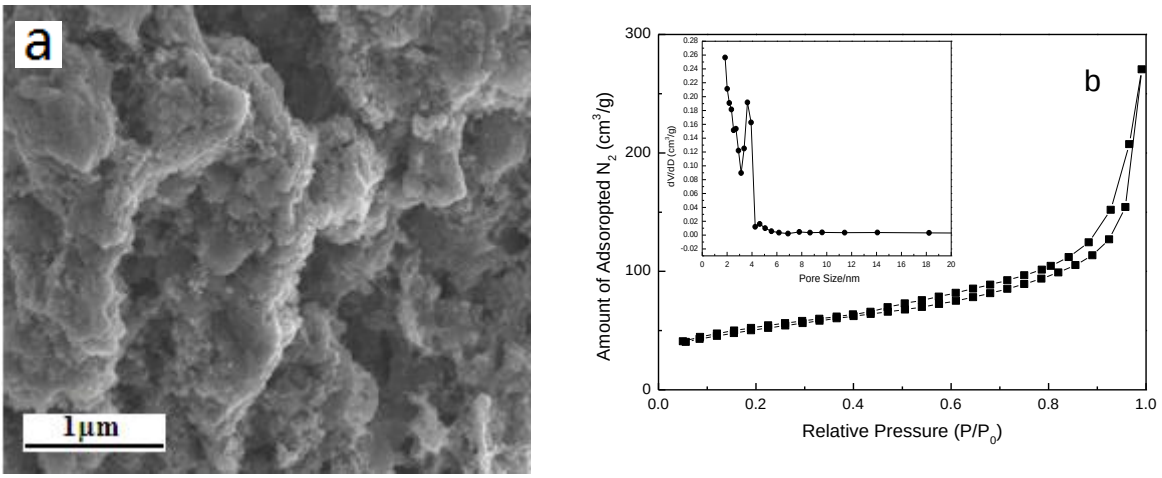

Figure 2. SEM image (a) and N_2 adsorption-desorption isotherm (the inset shows the pores size distribution) (b) of Al_2O_3 template.

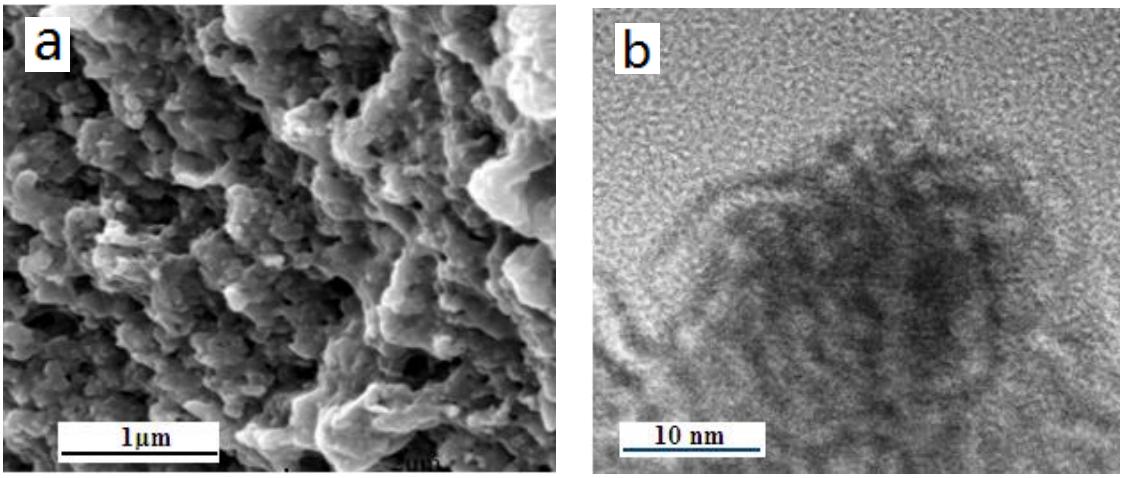

Figure 3. SEM (a) and TEM (b) images of 3D MnO_2 sponge

The SEM and TEM images of the as-prepared MnO_2 massive particles are shown in Fig.3a and b, respectively. The SEM image reveals that sponge MnO_2 monoliths consist of aggregated nanostructure with clearly observable holes. The jagged morphology is characteristic of the Al_2O_3

template. The TEM image further indicates that the aggregated nanostructure is composed of worm-like entangled nanofibers which are the duplication of Al_2O_3 template's mesopores. These results indicates that Mn^{2+} can penetrate into the pores of Al_2O_3 template when Al_2O_3 templates are put into the $MnCl_2$ solution and absorbed in nanopores of Al_2O_3 template when Al_2O_3 templates are separated from the $MnCl_2$ solution by filtration. The MnO_4^- anions will react with Mn^{2+} to produce MnO_2 in the nanopores of Al_2O_3 template and these nanopores become the microreactors for MnO_2 generation. Hence, the pores of Al_2O_3 template are successfully duplicated. The formation mechanism of 3D MnO_2 is similar to that of 1D carbon nanofiber from a sacrificial template[27]. Compared 1D or 2D nanostructures[16, 23, 24], Such 3D sponge morphology of the as-prepared MnO_2 with nanofibers is highly preferable for electrochemical application because the electrolyte ions could penetrate the pores to reach the inner electroactive sites and it will also own an excellent structure stability.

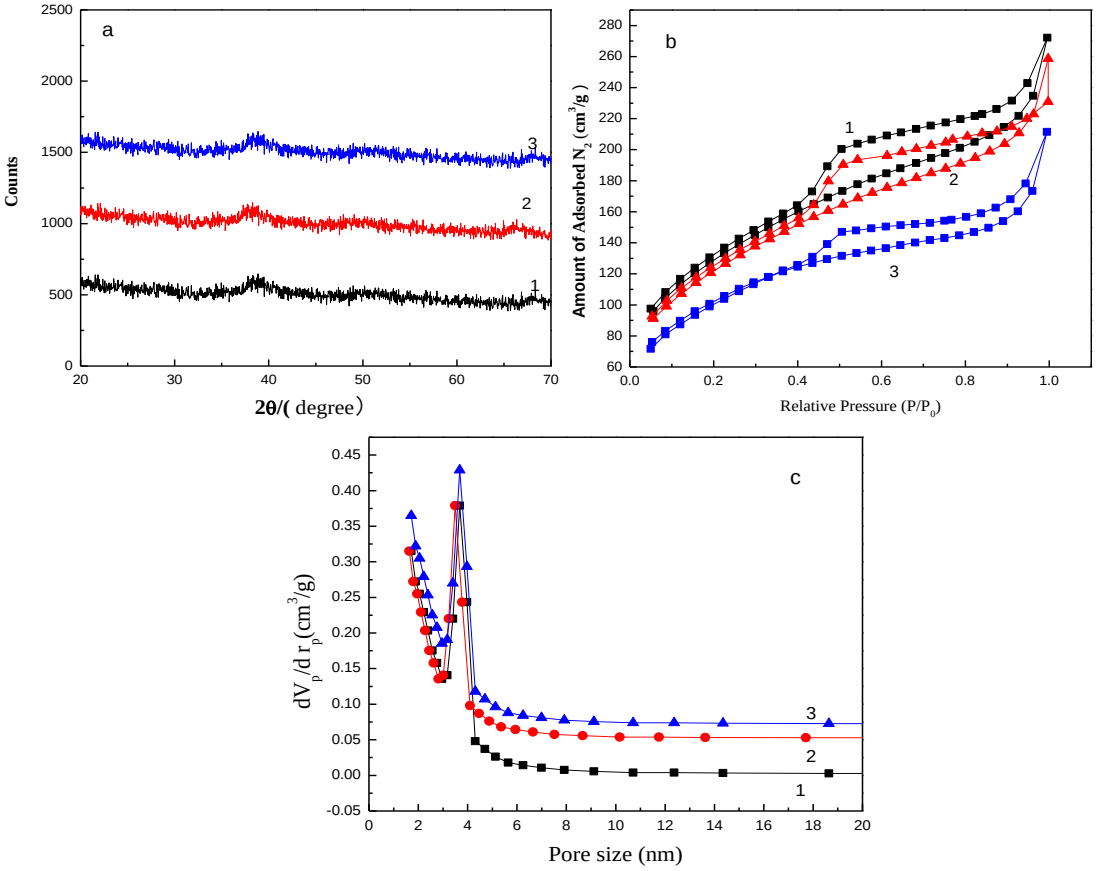

Figure 4. XRD patterns (a), N_2 adsorption-desorption isotherms (b) and pore size distribution of MnO_2 sponge obtained with different concentration of $MnCl_2$ solution. 1, 0.02mol L^{-1}; 2, 0.1mol L^{-1}; 3, 1mol L^{-1}.

The XRD patterns of the as-prepared MnO_2 with different concentration of $MnCl_2$ solution to immerse Al_2O_3 template are displayed in Fig.4a. All the samples have similar XRD patterns, with weak and broad peaks around $2\theta = 37.7$ and 66^0, indicating that all the formed MnO_2 is poorly crystalline[8]. The similar XRD patterns of MnO_2 obtained from different conditions also reveals that the formation

mechanism of MnO_2 doesn't change with the concentration of Mn^{2+} solution. Fig.4b is the nitrogen adsorption-desorption isotherms of MnO_2 synthesized with different concentration of $MnCl_2$ solution. All samples show very similar adsorption-desorption characteristics. The hysteresis loop in the relative pressure (P/P_0) rage of 0.45 to 0.95 indicates the presence of a mesoporous structure. The specific areas and the calculated specific volumes for samples obtained in different preparation conditions are collected in Table 1. Although the concentration of the starting material (Mn^{2+}) doesn't change the characteristic of pore structure, it does change the specific surface area of the as-prepared MnO_2. The calculated specific surface area of the MnO_2 sample prepared from 0.02mol L^{-1} $MnCl_2$ solution is 456.9 m^2 g^{-1}. When the concentration of $MnCl_2$ solution increases to 0.1 and 1 mol L^{-1}, the specific surface area of the obtained MnO_2 changes to 365.5 and 319.8 m^2 g^{-1}, respectively. The reduction of the specific surface area of the as-prepared MnO_2 indicates that higher concentration of starting material will leave larger amount of Mn^{2+} in the pores of Al_2O_3 template, producing higher density of MnO_2 nanofiber. Fig4.c is the BJH pore-size distribution calculated from the isotherm. When the concentration of $MnCl_2$ solution increases from 0.02 to 1 mol L^{-1}, the pore characteristic of the as-prepared MnO_2 doesn't change greatly except the amounts of pores. The pore size is almost around 4.0nm and the pore volume is ca. 0.37cm^3 g^{-1} when the concentration of $MnCl_2$ solution is low (0.02mol L^{-1}). With the increase of the starting material's concentration to 0.1 and 1 mol L^{-1}, pitifully, the pore volume reduces to 0.25 and 0.23 cm^3 g^{-1} respectively, and the pore size distribution of the as-prepared MnO_2 becomes broader. The reduction of both specific surface area and pore volume indicates that the amount of the starting material in pores of Al_2O_3 template is an effective factor to adjust the characteristic of the as-prepared MnO_2 which is expected to affect its electrochemical performance for supercapacitor application.

Table 1. The specific area and the calculated specific volume for different samples

The concentration of Mn^{2+} (mol L^{-1})	0.02	0.1	1
pore size (nm)	3.9	3.9	3.9
Specific surface area (m^2 g^{-1})	456.9	365.5	319.8
Specific pore volume(cm^3 g^{-1})	0.37	0.25	0.23

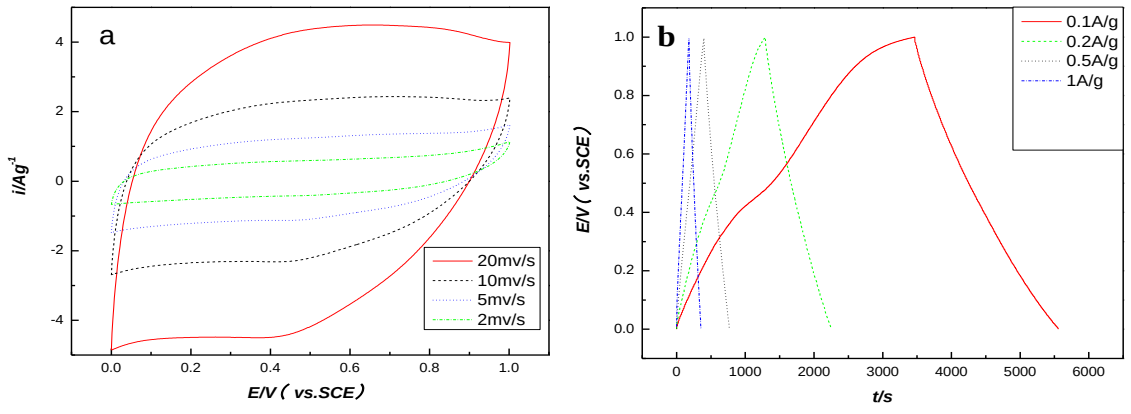

Figure 5. the CV curves and charge-discharge curves of typical 3D MnO_2 sponge electrode

Fig.5a shows the typical cyclic voltammogram of the as-prepared 3D MnO_2 at various scan rates in the potential range between 0 and 1.0V (versus SCE). All voltammograms are nearly rectangular mirror images with respect to the zero-current line, revealing that the electrode made from 3D MnO_2 is charged and discharged at pseudoconstant rate throughout the voltammetric cycle and shows a perfect electrochemical capacitive behavior [8, 28]. The pair of redox peaks appears in each CV curves indicates that the charge storage of as-prepared MnO_2 involves the intercalation / deintercalation of H^+ or M^+ into the oxide particle which often occur within the near-surface region except for the adsorption/desorption of protons(H^+) or alkaline cations (M^+) on MnO_2 surface [8. 29]. Fig.5b shows galvanostatic charge-discharge behaviors of the as-prepared MnO_2 sponge electrode at different current densities in a potential range of 0-1.0V versus SCE. Both charge and discharge portions remain approximately symmetric and linear, also indicating that 3D MnO_2 electrode has good capacitive behaviors. However, the slight voltage plateau in charge portion indicates that the 3D MnO_2 electrode behaves like a galvanic cell. This result may be resulted from that the highly strained nanoparticles in 3D nanofiber sponge enhance surface adsorption and facilitate the faradaic reaction[29]. Even though, the 3D MnO_2 electrode behaves like a capacitor rather than a galvanic cell and can be used in the so-called pseudocapacitor. Both CV tests and chronopotentiometry results reveal that the as-prepared porous MnO_2 sponge using mesoporous Al_2O_3 as sacrificial template is suitable for active electrode materials for supercapacitors. The specific capacitances of 3D MnO_2 electrodes from different concentration of Mn^{2+} solution calculated from CV curves are summarized in Fig.6. At the scan rate of 2mV s^{-1}, the MnO_2 sponge sample from 0.02mol L^{-1} Mn^{2+} solution provides a maximum capacitance value of 215.3 F g^{-1}, which may be ascribed to its highest specific surface area and porosity. With the increase of scan rates, the capacitance value of the obtained MnO_2 decreases, indicating that the higher charge transfer resistance exists at high scan rates. Even this, the as-prepared 3D MnO_2 sponge with low concentration of Mn^{2+} solution shows the best rate capability(, revealing the best electrochemical performance for supercapacitor applications.

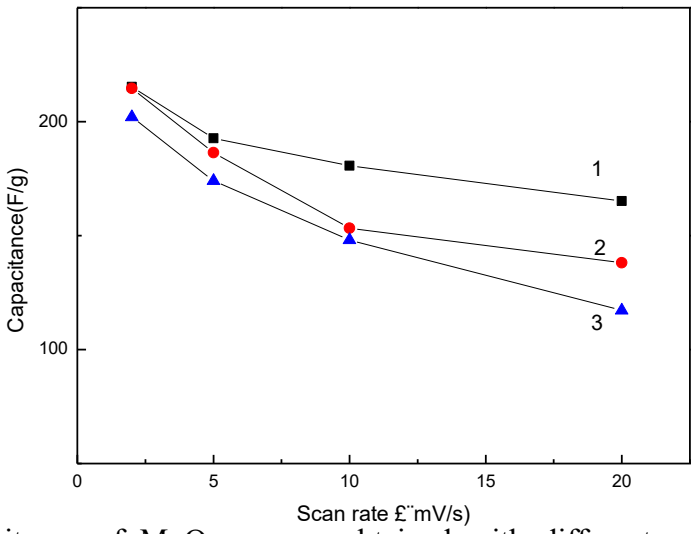

Figure 6. Specific capacitance of MnO_2 sponge obtained with different concentration of $MnCl_2$ solution. 1, 0.02mol L^{-1}; 2, 0.1mol L^{-1}; 3, 1mol L^{-1}.

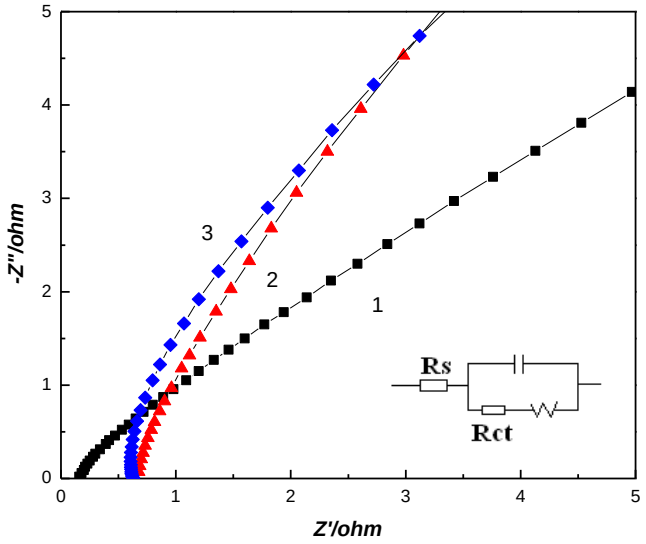

Figure 7. Nyquist plots for MnO_2 prepared with different concentrations of manganese chloride (1: 0.02mol L^{-1}, 2: 0.1mol L^{-1}, 3: 1mol L^{-1})

Fig.7 shows the Nyquist plots for the as-prepared 3D MnO_2 sponge electrodes from different concentration of Mn^{2+} solution, where Z' and Z'' are the real and imaginary parts of the impedance, respectively. The inset in Fig.7 displays the equivalent circuit diagram used for the EIS fitting. For all the MnO_2 electrodes, no obvious semicircle can be seen at high frequencies except a straight line at low frequencies. The semicircle represents the charge transfer resistance (R_{ct}) at the electrode/electrolyte interface which is related to the electronic resistance within the electrode materials [8, 18]. The less obvious semicircle at high frequencies indicates that the obtained MnO_2 electrode has a fast charge transfer ability (R_{ct} is very small), which benefits to the capacitive performance[8, 30, 31]. The straight line at lower frequency region (Warburg, W) can be attributed to the diffusion process at the electrode/electrolyte interface. Compared to the line at lower frequency for 3D MnO_2 electrode obtained from 0.02 mol L^{-1} Mn^{2+}, the vertical line at lower frequencies for the 3D MnO_2 electrodes obtained from higher concentration of Mn^{2+}(0.1 and 1 mol L^{-1} $MnCl_2$) represents the easier ion diffusion in the structure, indicating a more ideal capacitance behavior[17, 22, 32]. This result may be due to the existence of larger pore in the samples obtained from higher concentration(see Fig.4c). however, the estimated equivalent resistance, R_s (which is combination of ionic resistance of the electrolyte, intrinsic resistance of active materials and contact resistance at he active materials-current collector interface) for MnO_2 sample prepared from low concentrated Mn^{2+} solution is much lower than that of MnO_2 samples obtained from other thicker concentrated Mn^{2+} solution, indicating a better charge movement in this electrode[8, 17, 33]. As shown in Fig.7, The fast kinetics of MnO_2 sponge electrode may be ascribed to the nanofiber characteristic in porous MnO_2 foam, which provides more electrochemically active surface area for reversible faradaic reaction by shorten the path for ion diffusion.

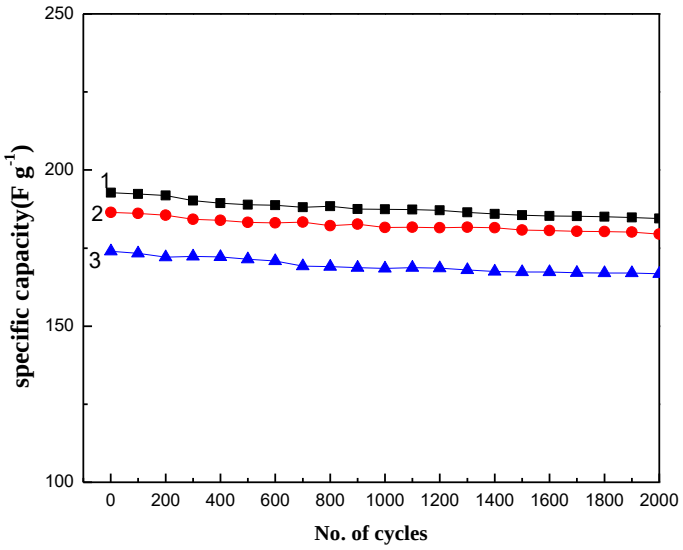

Figure 8. Variation of the specific capacitance for MnO_2 electrode prepared with different concentrations of manganese chloride as a function of the number of cycles. 1: 0.02mol L^{-1}, 2: 0.1mol L^{-1}, 3: 1mol L^{-1}

Table 2. electrochemical performance of 3D MnO_2 sponge in comparison with electrodes based on different MnO_2 nanostrures reported in the literature

Type of materials	Specific capacitance	Cycling stability	references
MnO_2 nanowires	590 F g^{-1} at 10mV s^{-1}	80.9% after 2000 cycles	[34]
MnO_2 nanowires	50-70 F g^{-1} at 1-5 mV s^{-1}	less than 97% after 1000 cycles	[35]
MnO_2 nanorods	185 F g^{-1} at 1A g^{-1}	less than 91% after 1000 cycles	[16]
MnO_2 nanosheets	121F g^{-1} at 1A g^{-1}	71.4% after 3000 cycles	[36]
MnO_2 spheres	188-203 F g^{-1} at 2mV s^{-1}	-	[37]
Flower-like MnO_2	495 F g^{-1} at 1A g^{-1}	91% after 1000 cycles	[16]
Flower-like MnO_2	150.9 F g^{-1} at 0.5A g^{-1}	90.28% after 1000 cycles	[38]
3D MnO_2 sponge	215.3 F g^{-1} at 2mV s^{-1}	more than 96% after 2000 cycles	our works

To extensively understand the electrochemical properties of as-prepared MnO_2 sponge materials, the cycling stability of the MnO_2 electrodes were also tested by CV at 5mV s^{-1} for 2000cycles and is presented in Fig.8. Through the various initial capacitances is obtained for different MnO_2 sponge, the capacitance retentions of all the MnO_2 electrodes excess more than 96% of their initial capacitance after 2000 cycles. Compared with the results of MnO_2 electrodes reported in litherature(Table 2), the MnO_2 nanofiber sponges electrode exhibits an excellent cycling stability even though its specific capacitance is not enough attractive. Good cycle life of MnO_2 nanofiber sponges electrode shows excellent chemical stability for the three-dimensional structure of the obtained MnO_2, further proving the promising potential of 3D MnO_2 sponge as active materials of supercapacitor electrodes.

4. CONCLUSIONS

3D MnO_2 Sponge composed of worm-like nanofiber was successfully prepared by redox reaction of Mn^{2+} and MnO_4^- using mesoporous Al_2O_3 as sacrificial template. Different concentrations of $MnCl_2$ solution was used to immerse the Al_2O_3 template and to prepare MnO_2 sponge. The structure and morphology of the resultant 3D MnO_2 were characterized by XRD, SEM, TEM and BET methods. The electrochemical performance of MnO_2 sponge was investigated by CV, chronopotentiometry and EIS. 3D MnO_2 sponge consists of entangled worm-like nanofibers and its physical and chemical properties are affected by the concentration of the starting material which immerses the holes of Al_2O_3 template. MnO_2 Sponge materials exhibit excellent charge transfer capability, high specific capacitance and excellent cyclic stability, showing promising properties as active electrode materials for supercapacitors.

THIS STUDY WAS FUNDED BY AUTHORS THEMSELVES. THE AUTHORS DECLARE THAT THEY HAVE NO CONFLICT OF INTEREST.

References

1. Y.P. Zhai, Y.Q. Dou, D.Y. Zhao, F.F. Pasquale, T.M. Richard, S. Dai. *Adv. Mater*., 23(2011) 4828
2. J.A. Lee, M.K. Shin, S.H. Kim, H.U. Cho, G.M. Spinks, G.G. Wallace, M.D. Lima, X. Lepro, M.E. Kozlov. R.H. Baughman, S. Kim. *Nat. Commun*., 4(2013) 1
3. X.H. Lu, M.H. Yu, G.M. Wang, Y.X. Tong, Y. Li. *Energy Environ. Sci*., 7(2014) 2160
4. Z. Gao, W.L. Yang, J. Wang, N.N. Song, X.D. Li. *Nano Energy,* 13(2015) 306
5. M.F. EI-Kady, V. Strong, S. Dubin, R.B. Kaner. *Science*, 335(2012) 1326
6. M.M. Vadiyar, S.C. Bhise, S.K. Patil, S.A. Patil, D.K. Pawar, A.V. Ghule, P.S. Patil, S.S. Kolekar. *RSC Adv*., 5(2015) 45935
7. R.S. Diggikar, D.J. Late, B.B. Kale. *RSC Adv*., 4(2014) 22551
8. C.Y. Wan, L.Y. Yuan, X.R. Ye, F.H. Wu. *Electrochim. Acta,*147(2014) 712
9. L.Y. Yuan, C.Y. Wan, X.R. Ye, F.H. Wu. *Electrochim. Acta,* 213(2016) 115
10. P. Simon, Y. Gogotsi. *Nature Mater*., 7(2008) 845
11. B.A. Mei, L. Pilon. *Electrochim. Acta*, 255(2017) 168
12. G.P. Wang, L. Zhang, J.J. Zhang. *Chem. Soc. Rev*., 41(2012) 797
13. X. Luo, J.Y. Yang, D. Yan, W. Wang. X. Wu, Z.H. Zhu. *J. Alloys compd*., 723(2017): 505
14. M. Li, M. Zhou, Z.Q. Wen, Y.X. Zhang. *J. Energy Storage,* 11(2017) 242
15. M. Toupin, T. Brousse, D. Belanger. *Chem. Mater.,* 16(2004) 3184
16. J. Chu, D.Y. Lu, J. Ma, M. Wang. X.Q. Wang, S.X. Xiong. *Mater. Lett.,* 193(2017) 263
17. G.A.M. Ali, M.M. Yusoff, E.R. Shaaban, K.F. Chong. *Ceram. Int*., 43(2017) 8440
18. Y.H. Ding, N. Zhang, J.Y. Zhang, X.R. Wang, J.Q. Jin, X.F. Zheng. Y.Z. Fang. *Ceram. Int*.,43(2017) 5374
19. L. Zhang, T.H. Li, X.L. Ji, Z.Y. Zhang, W.B. Yang, J.J. Gao, H. Li, C.Y. Xiong, A.L. Dang. *Electrochim. Acta*, 252(2017) 306
20. K. Xiao, J.W. Li, G.F. Chen, E.Q. Liu, N. Li, Y.Z. Su. *Electrochim. Acta*, 149(2014) 341
21. L.Y. Yuan, C.Y. Wan, L.L. Zhao. *Int. J. Electrochem. Sci.,* 10(2015) 9456
22. L. Khandare, S. Terdale. *Appl. Surf. Sci*., 418(2017) 22
23. Y.M. He, W.J. Chen, X.D. Li, Z.X. Zhang, J.C. Fu, C.H. Zhao, E.Q. Xie. *ACS nano*., 7(2013):174

24. G.X. Wang, Q.Q. Tang, H. Bao, X.W. Li, G.C. Wang. *J. Power Sources*, 241(2013) 231
25. C. Liu, T. Peng, C.L. Wang, Y. Lu, H.L. Yan, Y.S. Luo. *J. Alloys compd*., 720(2017) 86
26. X.F. Shang, X.G. Wang, W.X. Nie, X.F. Guo, X.J. Zou, W.Z. Ding, X.G. Lu. *J. Mater. Chem.,* 22(2012) 23806
27. H.J. Liu, X.M. Wang, W.J. Cui, Y.Q. Dou, D.Y. Zhao, Y.Y Xia. *J. Mater. Chem.,* 20(2010)4223
28. D.D. Zhao, Z. Yang, L.Y. Zhang, X.L. Feng, Y.F. Zhang. *Solid-state Lett*. 14(2011) A93
29. O.A . Vargas, A. Caballero, L. Hernan, J.Morales. *J. Power Sources*, 196(2011) 3350
30. P. Sen, A. De, A.D. Chowdhury, S.K. Bandyopadhyay, N. Agnihotri, M. Mukherjee. *Electrochim. Acta,* 108(2013) 265
31. S.H. Aboutalebi, A.T. Chidembo, M. Salari, K. Konstantinov, D. Wexler, H.K. Liu, S.X. Dou. *Energy Environ. Sci*., 4(2011) 1855
32. C.Y. Wan, L.Y. Yuan, H.Y. Shen. *Int. J. Electrochem. Sci.*, 9(2014) 4024
33. D.P. Dubal, D.S. Dhawale, R.R. Salunkhe, C.D. Lokhande. *J. Electrochem. Soc.*, 157(2010) A812
34. D.S. Patil, S.A. Pawar, J.C. Shin. *J. Ind. Eng. Chem.*, 62(2018) 166
35. L. Khandare, S. Terdale. *Appl. Surf. Sci.*, 418(2017) 22
36. Q.Q. Tang, M.Q. Sun, S.M. Yu, G.C. Wang. *Electrochim. Acta*, 125(2014) 488
37. A. Gambou-Bosca, D. Belanger. *Electrochim. Acta*, 201(2016) 20
38. J.Y. Dong, G. Lu, F. Wu, C.X. Xu, X.H. Kang, Z.M. Cheng. *Appl. Surf. Sci.,* 427(2018) 986